Inclusive low mass Drell-Yan production in the forward region at $\sqrt{s} = 7$ TeV

Jonathon Anderson[1] on behalf of the LHCb collaboration

[1]Physik-Institut der Universität Zürich, Switzerland.

DOI: `http://dx.doi.org/10.3204/DESY-PROC-2012-02/145`

A measurement of the Drell-Yan cross-section in dimuon final states for muons within pseudorapidities of 2 to 4.5, in the mass range $5 < \mathrm{M} < 120$ GeV/c^2, is presented. The muons are required to have a momenta larger than 10 GeV/c and a transverse momenta larger that 3 GeV/c. The cross section is measured differentially, in mass, and in rapidity of the virtual photon in two distinct mass regions. The analysis uses the full dataset collected by the LHCb experiment during 2010 with an integrated luminosity of 37 pb^{-1}.

1 Introduction

The LHCb detector [1] is a single-arm forward spectrometer at the LHC covering the pseudorapdity range $2 < \eta < 5$, primarily designed for the study of particles containing b or c quarks. In addition to its main flavor physics programme, LHCb can make precision measurements of electroweak bosons at high rapidities. This document describes measurements of the differential cross-section of low mass Drell-Yan production with the LHCb detector at $\sqrt{s} = 7$ TeV using about 37 pb^{-1} of data collected in 2010 [2].

These measurements are an important test of the Standard Model at LHC energies. Perturbative QCD predictions of these processes are available at next-to-next-to-leading order (NNLO). The measurements of the low mass Drell-Yan cross-sections at LHCb are sensitive to Bjorken-x values as low as 8×10^{-6} for four-momentum transfer $\mathrm{Q}^2 = 25$ GeV^2/c^4, where x is the momentum fraction carried by the struck quark. They will provide important input to the knowledge of the parton density functions and the understanding of the theoretical calculations.

2 Analysis overview

Candidate $\gamma^\star \to \mu\mu$ events are selected via a dimuon trigger and an offline selection that requires that each muon has momenta $\mathrm{p} > 10$ GeV/c, transverse momenta $\mathrm{p}_T > 3$ GeV/c, pseudorapidity $2 < \eta < 4.5$ and, combined, that the dimuon pair has an invariant mass in the range $5 < M_{\mu\mu} < 120$ GeV/c^2. The mass range $9 < M_{\mu\mu} < 10.5$ GeV/c^2, where the $\Upsilon \to \mu\mu$ contribution dominates, is excluded. While the high mass region is very pure, the background increases significantly towards low masses. Four sources of background have been evaluated: semileptonic decays of hadrons containing b and c quarks; pions and kaons that have been mis-identified as muons; $\gamma^\star/Z \to \tau\tau$ events where both taus decay to muons; and, for the mass bins below 10 GeV/c^2, the contribution due to the radiative tail of $\Upsilon \to \mu\mu$ events.

The signal yield is extracted by a template fit to the minimum muon isolation distribution of the two muons using the TFractionFitter ROOT package. Here the muon isolation is defined as the fraction of the transverse momenta of the muon-jet carried by the muon, $z = p_T^{\mu}/p_T^{Jet}$. The muon-jet is defined as the jet which contains the muon, and is reconstructed with the anti-kt algorithm [3] with the size R = 0.5. Signal events are expected to have an isolation distribution close to unity while the background events tend to have lower values since they are usually produced in the same direction as the other fragmentation products. Fits are performed in nine different mass bins and in five rapidity bins in two mass regions. The signal template used in the fits is obtained from simulation. This is validated by comparing the isolation distribution for $\Upsilon \to \mu\mu$ and $Z \to \mu\mu$ events in data and simulation where good agreement is seen. The template for backgrounds due to misidentified pions and kaons is obtained from data by taking opposite sign di-track combinations (assumed to be pions and kaons) in events that pass the minimum bias trigger and weighting each combination by the probability that both tracks are misidentified as muons. This probability is taken to be the fraction of tracks identified as muons in randomly triggered events and is parametrised as a function of the longitudinal momentum. The template for the heavy quark background is taken from data by selecting the events in our sample that have two muons that do not come from the proton-proton interaction vertex and do not form a common vertex. This sample also contains a contribution from $\gamma^{\star}/Z \to \tau\tau$ decays. For the mass bins below 10 GeV/c^2, a template describing the component due to the radiative tail of Υ decays is also included in the fit. This template is taken from simulation and the normalization in the fit is fixed to the number of expected Υ events extracted from a fit to the Υ mass distribution in data. The extracted sample purity varies between 7% and 100% depending on the mass and rapidity bin. To estimate the uncertainty on the fits due to our understanding of these templates, cross-check fits are performed using different templates. Here the mis-id template is taken from events containing two muons with the same charge, the heavy quark template is taken from simulation, and the signal template from simulation is distorted by applying a scale factor of 0.95 or 1.05. The resulting differences in the extracted signal yield are taken as the systematic uncertainties due to the template shapes. Here the largest uncertainty is due to the shape of the heavy quark template and varies depending on the mass bin, being 24% in the lowest mass bin and less than 1% for masses above 20 GeV/c^2.

The experimental efficiencies due to reconstruction and triggering are all determined from data using dimuon resonances (J/ψ, Υ and Z) and tag-and-probe techniques. The event yield is then corrected on an event by event basis as a function of the transverse momentum and pseudorapidity of the two muons. The systematic uncertainty on this correction is dominated by the uncertainty on the determination of the tracking efficiencies which is limited by the available statistics and varies between 4% and 10% depending on the mass and rapidity bin.

Two methods are used to determine the integrated luminosity, a Van der Meer scan [4] where the colliding beams are moved transversely across each other to determine the beam profile, and a beam gas method [5], where reconstructed beam-gas interaction vertices near the beam crossing point determine the beam profile. Both methods give similar results and have a precision of 3.5%.

Since the cross-section is measured in the kinematic range of the measurement, the only acceptance correction comes from migrations into and out of the phase space. The acceptance is determined from simulation and is consistent with one. Corrections are applied for bin-to-bin migrations. They are estimated from MC and found to be small, below 1% for most of the bins. No corrections are yet applied for final state radiation.

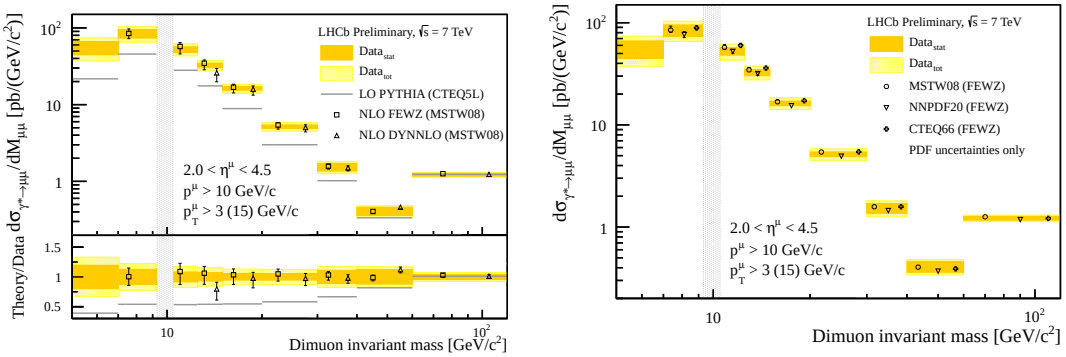

Figure 1: $\gamma^\star \to \mu\mu$ cross section as a function of dimuon mass. The orange bands correspond to the statistical uncertainties, the yellow band to the statistical and systematic uncertainties added in quadrature. (a): Superimposed are the PYTHIA predictions and the NLO predictions from FEWZ and DYNNLO. The lower plot shows the ratio of the predictions or the uncertainties to the data. (b): Superimposed are NLO predictions from FEWZ with the PDF sets from MSTW08, NNPDF and CTEQ. The uncertainties of the NLO predictions contain the PDF uncertainties evaluated at the 68% confidence level and the theoretical errors added in quadrature.

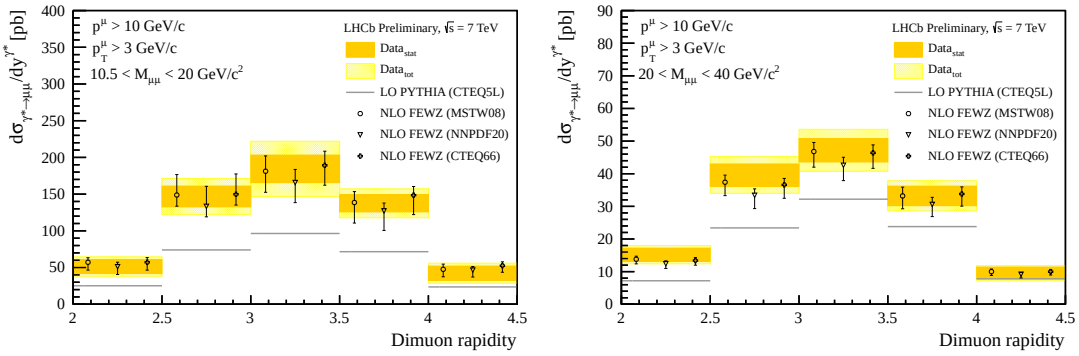

Figure 2: Differential cross section for $\gamma^\star \to \mu\mu$ as a function of rapidity for two different dimuon mass regions (a: $10.5 < M < 20 GeV/c^2$, b: $20 < M < 40 GeV/c^2$). The orange bands correspond to the statistical uncertainties, the yellow band to the statistical and systematic uncertainties added in quadrature. Superimposed are NLO predictions from FEWZ with the PDF sets from MSTW08, NNPDF and CTEQ; they are displaced horizontally for presentation. The NLO uncertainties correspond to the PDF uncertainties evaluated at the 68% confidence level.

3 Results

Figure 1(a) shows the differential cross-section as a function of the invariant mass of the dimuons together with predictions from PYTHIA [6] (normalised to the cross-section measured in the highest mass bin) and NLO calculations. NLO predictions are only available for FEWZ [7] for masses larger than 7 GeV/c^2 and for DYNNLO [8] for masses larger than 12.5 GeV/c^2. Figure 1(b) shows the same data in comparison with FEWZ predictions with three different PDF sets: MSTW08 [9], NNPDF20 [10] and CTEQ66 [11]. Here, only the uncertainties due to the PDF uncertainty is shown; these are smaller than the theory uncertainties at NLO. Figure 2 shows the differential cross-section as a function of the rapidity of the dimuons in two different mass bins. PYTHIA underestimates the Drell-Yan cross-section by more than a factor two but describes the shapes in y and mass reasonably well. The FEWZ predictions with three different PDFs describe all the shapes and also the normalisation over the mass region where the calculation is valid.

4 Conclusions

The Drell-Yan cross-section has been measured for dimuon invariant masses $5 < M_{\mu\mu} < 120$ GeV/c^2 using 37 pb^{-1} of data collected in 2010. The signal is extracted by fitting signal and background templates to the isolation distribution of the muons. At low masses the dominant systematic uncertainty comes from the uncertainty of the shapes of the templates. The cross-section is measured as a function of the invariant dimuon mass and as a function of the dimuon rapidity in two different invariant mass regions. While the PYTHIA predictions agree in shape but are too low in normalisation, reasonable agreement is found with NLO predictions in those mass regions where the calculations are available.

References

[1] The LHCb collaboration, *The LHCb Detector at the LHC*, JINST **3** S08005 (2008).

[2] The LHCb collaboration, *Inclusive low mass Drell-Yan production in the forward region at $\sqrt{s}$ = 7 TeV*, LHCb-CONF-2012-013.

[3] M. Cacciari and G. P. Salam, Dispelling the N3 myth for the k(t) jet-finder, Phys. Lett. B641 (2006) 57, arXiv:hep-ph/0512210.

[4] S. van der Meer, *Calibration of the effective beam height in the ISR*, ISR-PO/68-31, 1968.

[5] The LHCb collaboration, R. Aaij et al., *Absolute luminosity measurements with the LHCb detector at the LHC*, JINST 7 (2012) P01010, arXiv:1110.2866.

[6] T. Sjostrand, S. Mrenna, and P. Skands, PYTHIA 6.4 physics and manual, JHEP 05 (2006) 026, arXiv:hep-ph/0603175.

[7] R. Gavin, Y. Li, F. Petriello, and S. Quackenbush, FEWZ 2.0: A code for hadronic Z production at next-to-next-to-leading order, Comput. Phys. Commun. 182 (2011) 2388, arXiv:1011.3540.

[8] S. Catani, L. Cieri, G. Ferrera, D. de Florian, M. Grazzini, Phys. Rev. Lett. 103 (2009) 082001, arXiv:0903.2120.

[9] A. Martin, W. Stirling, R. Thorne, and G. Watt, Parton distributions for the LHC, Eur. Phys. J. C63 (2009) 189, arXiv:0901.0002.

[10] R. D. Ball et al., A first unbiased global NLO determination of parton distributions and their uncertainties, Nucl. Phys. B838 (2010) 136, arXiv:1002.4407.

[11] P. M. Nadolsky et al., Implications of CTEQ global analysis for collider observables, Phys. Rev. D78 (2008) 013004, arXiv:0802.0007.